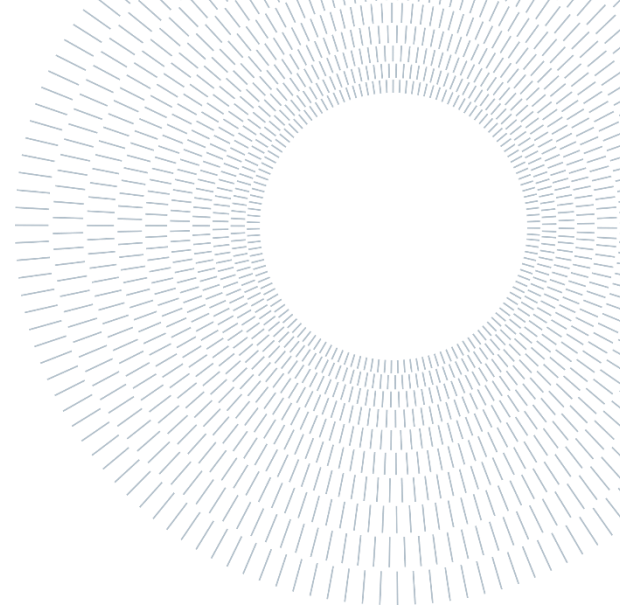




POLITECNICO
MILANO 1863

SCUOLA DI INGEGNERIA INDUSTRIALE
E DELL'INFORMAZIONE



EXECUTIVE SUMMARY OF THE THESIS

Operational analysis of a Surface-mounted Permanent Magnet Synchronous Machine subject to a fault in its stator winding

MASTER OF SCIENCE THESIS IN ELECTRICAL ENGINEERING – INGEGNERIA ELETTRICA

AUTHOR: DARIO HOTI

ADVISOR: PROF. ROBERTO PERINI

CO-ADVISOR: DR. ENG. MATTEO DEPONTI

ACADEMIC YEAR: 2023-2024

1. Introduction

Nowadays, permanent magnet synchronous machines are widely used due to their high efficiency and high power density.

These electric machines can experience various types of faults during their operational lifetime.

In the literature, several methods are being studied to detect each type of fault and to ensure prolonged operation of the machine after a fault, by confining the propagation of the faulty parts of the motor.

This objective is usually achieved by limiting the machine's performance compared to what it could provide during normal operation.

In this study, the machine analyzed is a Surface-mounted Permanent Magnet Synchronous Machine (SPMSM) subject to a fault in its stator winding that has already been identified:

specifically, a fault between adjacent turns in one of the coils that constitute the stator winding.

The objective of this study is to evaluate the performance of an SPMSM affected by a turn-to-turn short circuit fault that resulted in a coil-to-ground fault. Here, the parallel path containing the faulty coil is disconnected to preserve the machine operation at reduced performance, thereby temporarily delaying the machine shut down for maintenance purposes.

Also the performance of the machine in case of the symmetrical disconnection of one parallel path per each phase is examined to observe the difference from the case in which only the parallel path of the faulty phase is disconnected.

The study is structured by initially presenting an overview of the state-of-the-art of some possible fault-tolerant control strategies for a permanent magnet synchronous machine subject to a fault in the stator winding.

Subsequently, the constructive details of the machine and connection diagrams are presented, followed by an introduction to the circuit model of the permanent magnet.

This thesis analyses the magnetomotive forces over the thickness airgap + permanent magnets for each operational case:

- 1) Healthy machine;
- 2) Machine with faulty parallel path disconnected;
- 3) Machine with faulty parallel path and one parallel path per each of the remaining phases symmetrically disconnected.

The study continues by first analyzing the coil, couple of coils and phase magnetomotive forces over the airgap + magnets thickness to obtain the expressions of the stator rotating magnetic fields.

Contemporarily, also the magnetomotive force due to the permanent magnets on the rotor over the airgap + magnets thickness is determined.

Subsequently, it is presented a methodology to derive the expressions of the rotating fields due to the rotor magnets and due to the stator winding over both the airgap and the permanent magnets thickness separately.

The separate analysis of the magnetomotive forces over each of these thicknesses (i.e. airgap and circular ring of permanent magnets) is ultimately useful for first calculating the total magnetic co-energy stored in the machine , necessary to evaluate the electromagnetic torque of the SPMSM in any condition.

The novelty proposed in this work consists in providing a methodology to evaluate analytically, in any post-fault winding configuration, the expression of the machine's electromagnetic torque.

2. Constructional details

The SPMSM considered in this work is a 10 pole and 12 slots machine characterized by a symmetrical three-phase winding with $a = 2$ parallel paths per each phase winding.

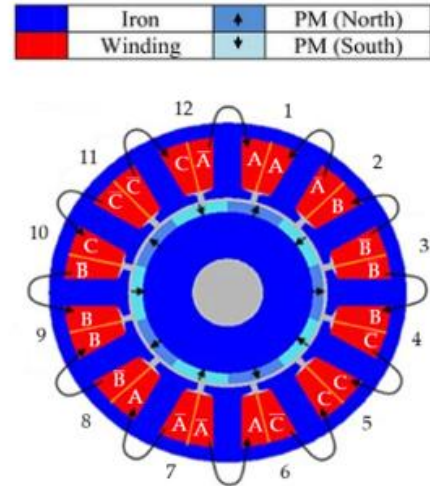


Figure 1: SPMSM with 10 poles and 12 slots

Each of the permanent magnets of the machine is shaped according to Figure 2.

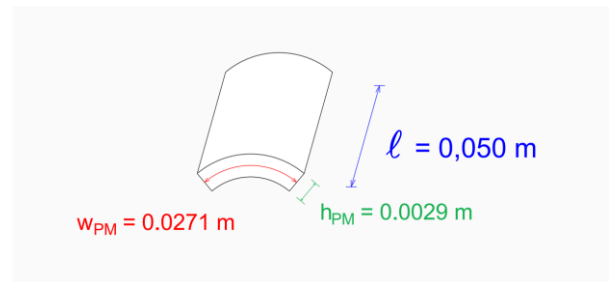


Figure 2: Shape and dimensions of each permanent magnet

The hysteresis loop of the permanent magnet in the second quadrant is approximated by the recoil line as shown in Figure 3.

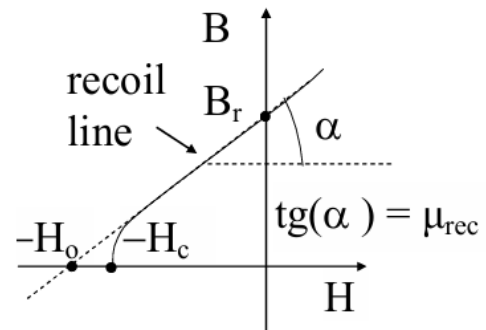


Figure 3: recoil line (i.e. approximated characteristic of the actual hysteresis curve of the permanent magnet in the II quadrant)

3. Equivalent circuit model of the permanent magnet

According to Figure 3, the actual hysteresis characteristic of the permanent magnet can be approximated by the recoil line of equation (1):

$$B = B_r + \mu_{rec} H \quad (1)$$

In which the slope of the recoil line is μ_{rec} , which is equal to the absolute magnetic permeability of the permanent magnet μ_{PM} .

Performing some calculations it can be found that the magnetomotive force of the permanent magnet measured between its external radial surfaces is equal to U_m :

$$U_m = H_0 \cdot h_{PM} - \frac{h_{PM}}{\mu_{PM} \cdot A_m} \cdot (B_m \cdot A_m) \quad (2)$$

In which:

- H_0 = absolute value of the intersection point between the recoil line and the H -axis;
- B_m = permanent magnet flux density;
- A_m = cross-section of the permanent magnet;
- h_{PM} = permanent magnet thickness.

In turn, eq. (2) can be viewed as eq. (3):

$$U_m = M_{PM} - \mathcal{R}_{PM} \cdot \Phi_{PM} \quad (3)$$

In which:

- M_{PM} = permanent magnet internal mmf;
- Φ_{PM} = permanent magnet flux;
- \mathcal{R}_{PM} = permanent magnet reluctance.

The equivalent circuit associated to eq. (3) is represented in Figure 4.

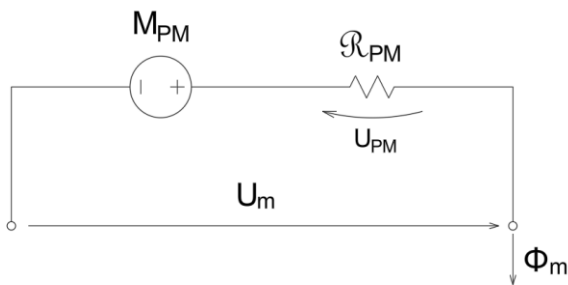


Figure 4: permanent magnet equivalent circuit

4. Definition of the stator reference frame and rotor reference frame

Defining two reference frames on the machine, one fixed with the stator and the other fixed with the rotor, it is possible to introduce the mechanical angular coordinates that measure the peripheral distance of a point with respect to each reference frame.

In Figure 5 can be observed the reference frames aforementioned:

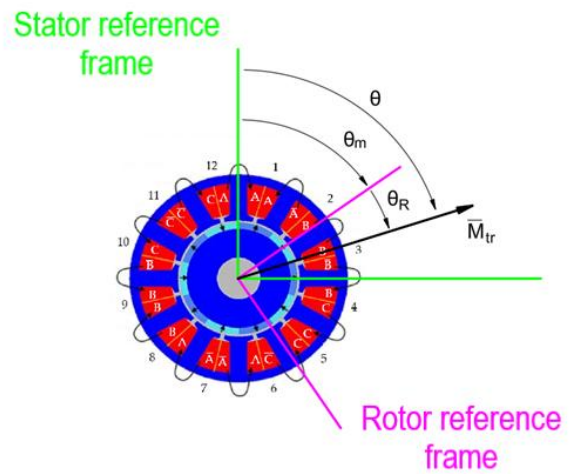


Figure 5: Stator reference frame and rotor reference frame

5. MMFs on the total width of airgap + circular ring of permanent magnets

In the following the expressions of some magnetomotive forces are derived on the width airgap + permanent magnets.

Assuming to represent the mmf as constant in front of the angular extension of each permanent magnet, the rotor mmf with respect to the rotor reference frame appears as in Figure 6.

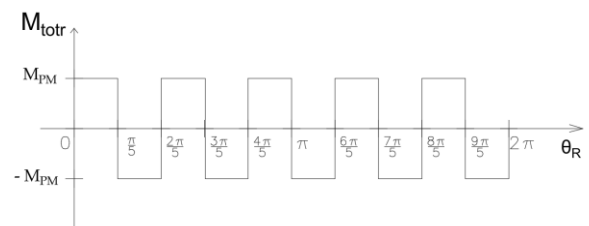


Figure 6: rotor mmf

From now on some plots are displayed concerning the mmfs with respect to the stator reference frame. The coil mmf $M_{BOBINA}(\theta)$ has the shape shown in Figure 7.

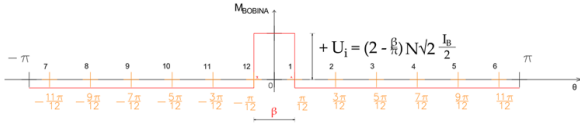


Figure 7: coil mmf $M_{BOBINA}(\theta)$

It can be seen that the amplitude of the coil mmf in the part of the periphery internal to the coil pitch β is higher than in the part of the periphery external to the coil pitch β . Instead, the mmf of a couple of coils with a common active side in the same slot $M_{\alpha}(\theta')$ has the shape shown in Figure 8.

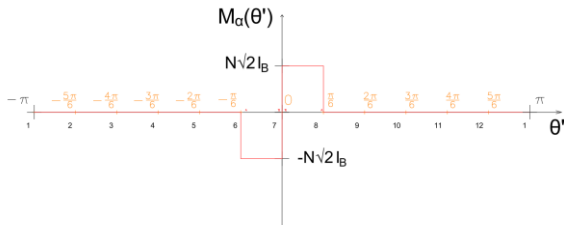


Figure 8: mmf of a couple of coils with a common active side in the same slot $M_{\alpha}(\theta')$

It can be seen that the shape of the mmf of a couple of coils is characterized by two rectangular half waves of equal amplitude.

Considering these two plots, the Fourier series expansion of both $M_{BOBINA}(\theta)$ and $M_{\alpha}(\theta')$ is determined.

Starting from the knowledge of $M_{BOBINA}(\theta)$ and from the position of all the coils connected in a certain phase, it is possible to determine the Fourier series expansion of that phase mmf on the thickness airgap + magnets.

The formula to obtain the Fourier series expansion of a certain phase mmf is:

$$M_{tsj}(\theta) = \sum_{i=1}^{N_c} M_{BOBINA,i}(\theta) \quad (4)$$

In which:

- j = generic phase A, B, C;
- i = i -th coil;
- N_c = number of coils per phase.

When one parallel path of a certain phase is disconnected, that phase mmf is equal to the couple of coils mmf or to the opposite of it, shifted accordingly to the position of its transition point from south pole to north pole.

In case of healthy machine the phase mmfs have the following shape:

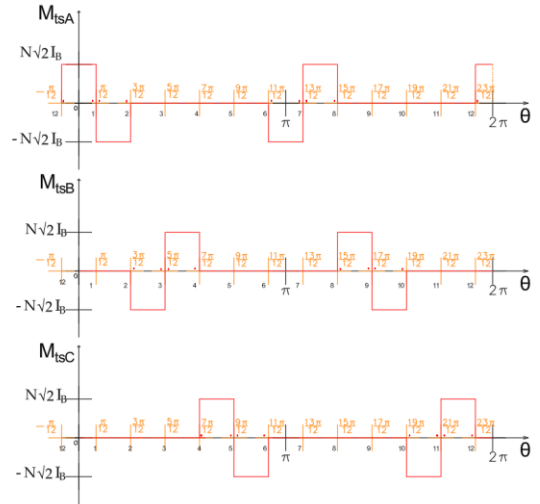


Figure 9: phase mmfs (healthy machine)

Instead, in case of one parallel path in phase A disconnected (i.e. parallel path a_1), the phase mmfs have the following shape:

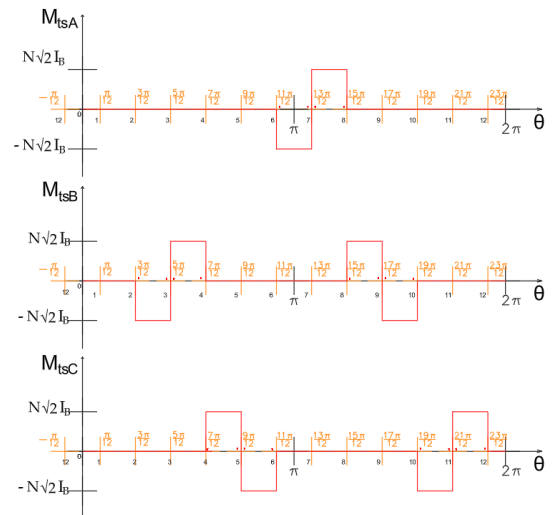


Figure 10: phase mmfs (with parallel path a_1 disconnected)

Instead, in case of one parallel path per each phase symmetrically disconnected (i.e. parallel paths a_1 , b_2 , c_1), the phase mmfs have the following shape:

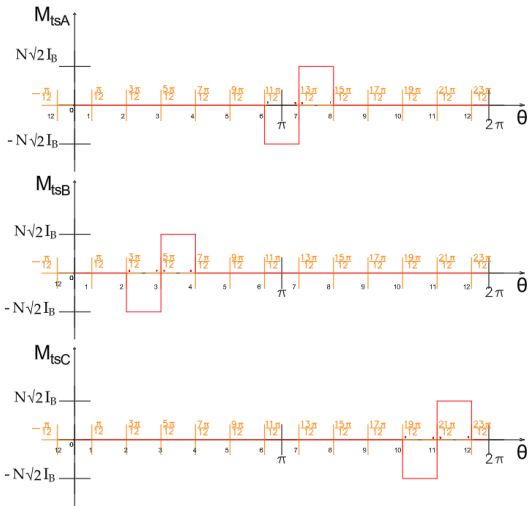


Figure 11: phase mmfs (with parallel paths a1, b2, c1 disconnected)

The winding factor of a certain phase with both of the parallel paths connected k_{wh} , expressed in function of the harmonic index h , is shown in Figure 12:

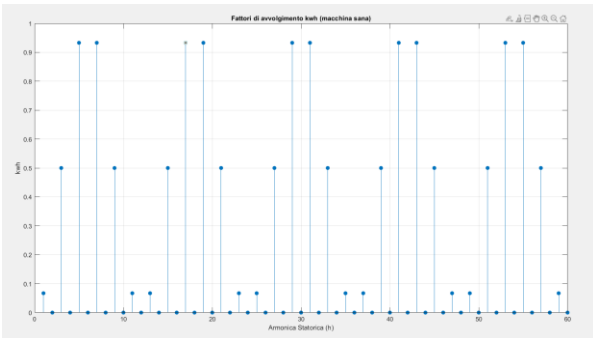


Figure 12: k_{wh} with both of the parallel paths connected

Observing Figure 12, it can be seen that all the even harmonics are null, therefore the phase mmf of a phase with both parallel paths connected is characterized by only odd harmonics.

Instead, if one parallel path is disconnected:

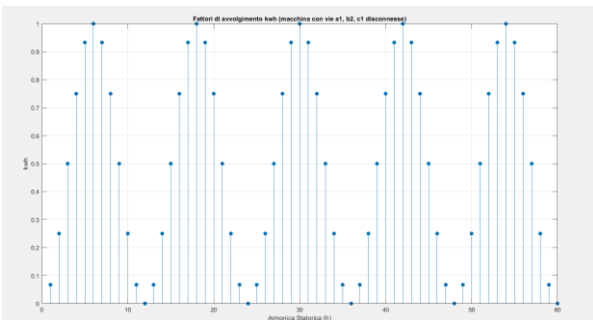


Figure 13: k_{wh} with one parallel path disconnected

Figure 13 shows that if one parallel path of a certain phase is disconnected, the phase mmf is characterized also by even harmonics.

The winding factor of the main harmonic $h = 5$ is unchanged after the disconnection of one parallel path, but the phase mmf is lower due to the lower number of coils per phase connected and due to the need to lower the phase current after the disconnection of one parallel path

6. Stator rotating MMFs on the total width of airgap + circular ring of permanent magnets

Feeding the three-phase winding with a set of three-phase balanced sinusoidal currents, the total stator mmf $M_{ts}(\theta, t)$ is calculated as:

$$M_{ts}(\theta, t) = M_{tsA}(\theta, t) + M_{tsB}(\theta, t) + M_{tsC}(\theta, t) \quad (5)$$

In which $M_{ts}(\theta, t)$ is static in space but time varying.

In turn, $M_{ts}(\theta, t)$ can be interpreted as produced by the simultaneous presence of two counter rotating stator mmf fields: the direct rotating stator field $M_{ts}^+(\theta, t)$ and inverse rotating stator field $M_{ts}^-(\theta, t)$, depending if the field rotates in the same measurement direction of θ or not.

Hence, the Fourier series expansion of the direct and inverse rotating stator fields is obtained for each operational condition of the machine concerning the parallel paths connected or disconnected.

The amplitude of the harmonics of the stator rotating fields in the airgap + magnets width is M_{tsh}^+ for the direct rotating field and M_{tsh}^- for the inverse rotating field.

7. Rotor rotating MMFs on each width airgap and circular ring of permanent magnets

To determine how the total rotor rotating field on the width airgap + magnets $M_{Lotr}(\theta, t)$ is shared between airgap and circular ring of permanent magnets, we must consider how the flux produced by each permanent magnet flows inside the machine. This representation is provided in Figure 14.

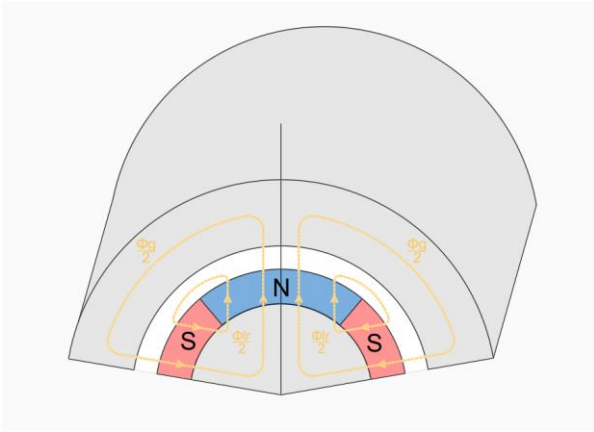


Figure 14: Bifurcation of each permanent magnet flux in the airgap

Observing the Figure 14, the equivalent magnetic circuit seen by the flux lines produced by each permanent magnet is shown in Figure 15.

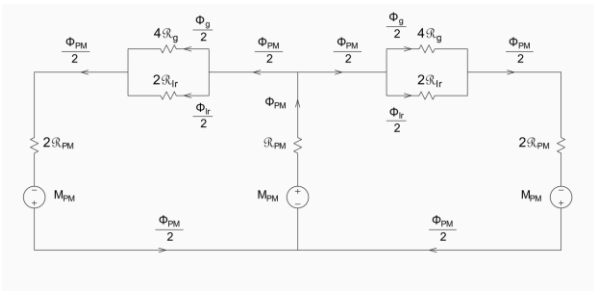


Figure 15: Equivalent magnetic circuit of the permanent magnet flux ϕ_{PM}

It is of interest the determination of the air gap rotor rotating mmf and of the rotor rotating mmf on the circular ring of permanent magnets. To determine the harmonic amplitude of each of these fields, it is needed the mmf of the permanent magnet on its external terminals U_m and the magnetic potential drop of the permanent magnet on its internal reluctance \mathcal{R}_{PM} .

8. Stator rotating MMFs on each width airgap and circular ring of permanent magnets

To determine how the direct rotating and inverse rotating stator fields on the width airgap + magnets $M_{ts}^+(\theta, t)$ and $M_{ts}^-(\theta, t)$ share between airgap and circular ring of permanent magnets, it should be considered how the flux produced by each stator coil flows inside the machine. This situation is illustrated in Figure 16.

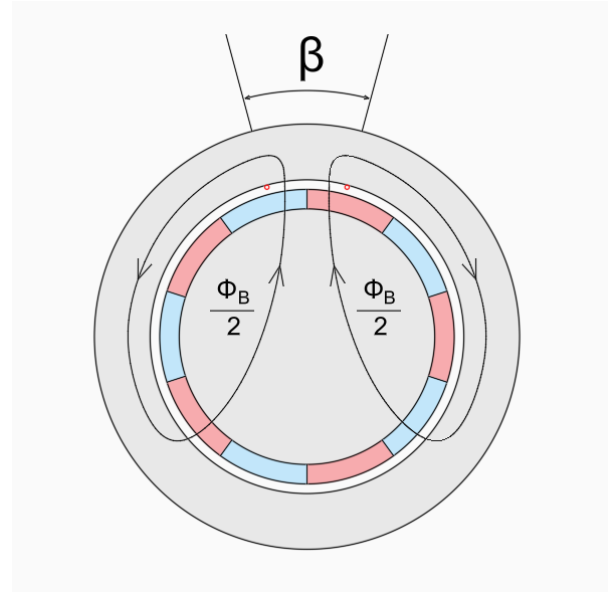


Figure 16: Bifurcation of the coil flux around its magnetic axis

The magnetic equivalent circuit seen by the coil flux lines is shown in Figure 17.

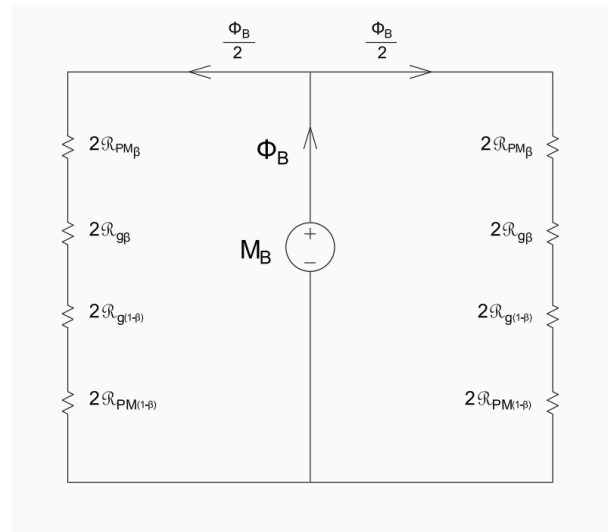


Figure 17: Equivalent magnetic circuit of the stator coil flux ϕ_B

In which:

$\mathcal{R}_{PM\beta}$ = reluctance of the sector of magnets internal to the coil pitch β ; $\mathcal{R}_{g\beta}$ = reluctance of the sector of airgap internal to the coil pitch β ; $\mathcal{R}_{g(1-\beta)}$ = reluctance of the sector of airgap external to the coil pitch β ; $\mathcal{R}_{PM(1-\beta)}$ = reluctance of the sector of magnets external to the coil pitch β ; M_B is the coil mmf.

The equivalent circuit in Figure 17 can be redrawn as in Figure 18.

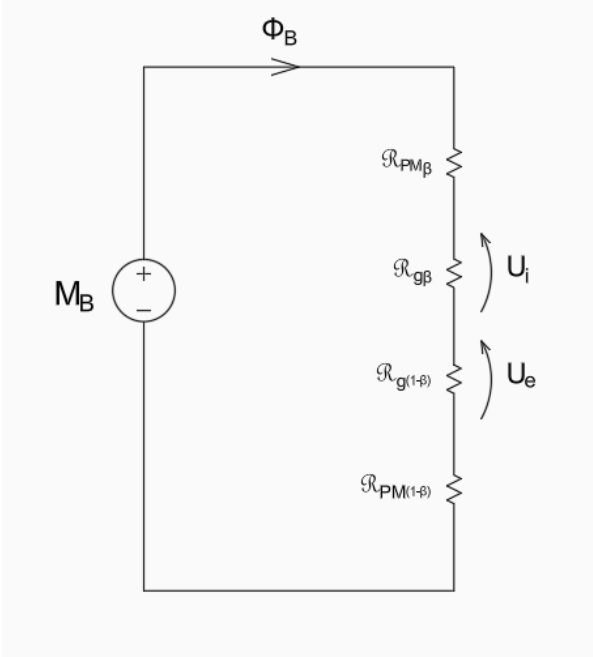


Figure 18: Magnetic potential drops of the coil mmf in the airgap internal to the coil pitch U_i and in the airgap external to the coil pitch U_e

In which U_i is given by:

$$U_i = \frac{\mathfrak{R}_{g\beta}}{\mathfrak{R}_{PM\beta} + \mathfrak{R}_{g\beta} + \mathfrak{R}_{g(1-\beta)} + \mathfrak{R}_{PM(1-\beta)}} \cdot M_B \quad (6)$$

By defining a parameter ε given by the ratio of reluctances in (6):

$$\varepsilon = \frac{\mathfrak{R}_{g\beta}}{\mathfrak{R}_{PM\beta} + \mathfrak{R}_{g\beta} + \mathfrak{R}_{g(1-\beta)} + \mathfrak{R}_{PM(1-\beta)}} \quad (7)$$

It can be found the parameter τ that determines the share of the rotating fields on the width airgap + magnets $M_{ts}^+(\theta, t)$ and $M_{ts}^-(\theta, t)$ that is present only in the air gap.

$$\tau = \frac{2}{\left(2 - \frac{\beta}{\pi}\right)} \cdot \varepsilon \quad (8)$$

The expression of the harmonic amplitudes of the direct and inverse stator rotating fields in the airgap is:

$$\begin{cases} M_{tsgh}^+ = \tau \cdot M_{tsh}^+ \\ M_{tsgh}^- = \tau \cdot M_{tsh}^- \end{cases} \quad (9)$$

Instead, the expression of the harmonic amplitudes of the direct and inverse stator rotating fields in the circular ring of permanent magnets is:

$$\begin{cases} M_{tsPMh}^+ = (1 - \tau) \cdot M_{tsh}^+ \\ M_{tsPMh}^- = (1 - \tau) \cdot M_{tsh}^- \end{cases} \quad (10)$$

9. Total magnetic coenergy stored in the machine

The assumptions adopted to present the methodology in the present thesis are:

- Negligible magnetic potential drops both in the stator core and in the rotor core due to the magnetic permeability of such structures $\mu_{fe} \rightarrow \infty$;
- The coil leakage flux is neglected for simplicity;
- The rotor rotates in the direct direction at constant mechanical angular speed Ω_m ;
- The machine operates in steady-state conditions.

Due to the previous assumptions, since the magnetic potential drops on stator and rotor are negligible, the SPMSM machine has magnetic coenergy only in two regions:

- Airgap;
- Circular ring of permanent magnets;

Therefore, the total coenergy in the machine W_{μ}' , expressed in function of the coenergy in the airgap W_{μ_g}' and in function of the coenergy in the circular ring of permanent magnets $W_{\mu_{PM}}'$ is:

$$W_{\mu}' = W_{\mu_g}' + W_{\mu_{PM}}' \quad (11)$$

In which the airgap coenergy W_{μ_g}' is:

$$W_{\mu_g}' = \frac{\mu_0 \cdot D_g \cdot l}{4g} \cdot \int_0^{2\pi} F_g^2(\theta, t) d\theta \quad (12)$$

Instead, the coenergy in the circular ring of permanent magnets $W_{\mu_{PM}}'$ is:

$$W_{\mu_{PM}}' = \frac{\mu_{PM} \cdot D_{PM} \cdot l}{4h_{PM}} \cdot \int_0^{2\pi} F_{PM}^2(\theta, t) d\theta \quad (13)$$

The meaning of the quantities that appear in (12) and (13) is explained in the following:

μ_0 = vacuum magnetic permeability; D_g = average diameter of the airgap; l = axial length of the machine; g = airgap width; $F_g(\theta, t)$ = resultant mmf in the airgap; μ_{PM} = absolute magnetic permeability of the permanent magnet; D_{PM} = average diameter of the circular ring of permanent magnets; h_{PM} = width of the circular ring of permanent magnets;

$F_{PM}(\theta, t)$ = resultant mmf in the circular ring of permanent magnets.

From the expression of the total coenergy (11), the electromagnetic torque C_e can be found by expression (14):

$$C_e = \left. \frac{\partial W'_\mu}{\partial \theta_{m0}} \right|_{i_a, i_b, i_c = const.} \quad (14)$$

In which:

θ_{m0} is the initial mechanical angle ($t=0$) between the stator reference frame and the rotor reference frame and it is used to emulate a virtual infinitesimal mechanical rotation of the rotor (virtual work principle);

i_a, i_b, i_c are the phase currents and they are kept virtually constant to derive the expression of the electromagnetic torque, which is equivalent to the condition in which the time t is kept virtually frozen.

For each case concerning the parallel paths connected, the electromagnetic torque spectrum due to the stator direct rotating field C_{eh}^{*+} and inverse stator rotating field C_{eh}^{*-} is shown in the following Figures.

In case of healthy machine see Figures 19 and 20.

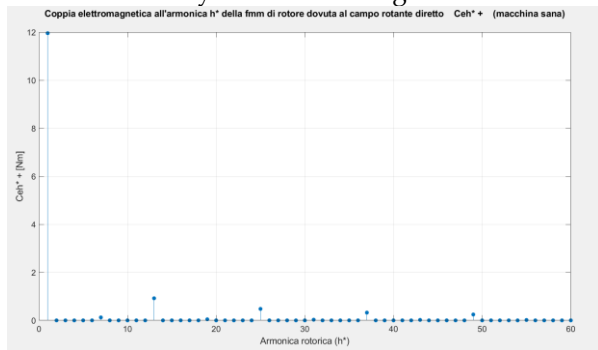


Figure 19: Torque spectrum C_{eh}^{*+} (Healthy machine)

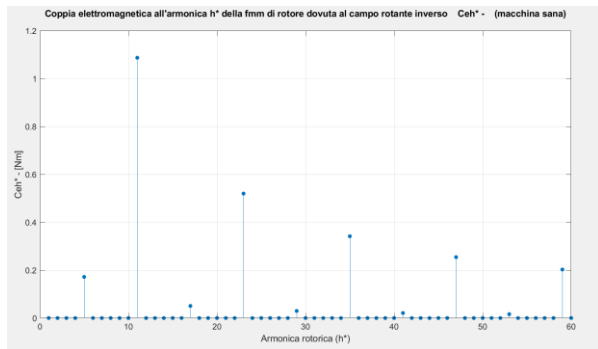


Figure 20: Torque spectrum C_{eh}^{*-} (Healthy machine)

In case of machine with one parallel path of only one phase disconnected see Figures 21 and 22.

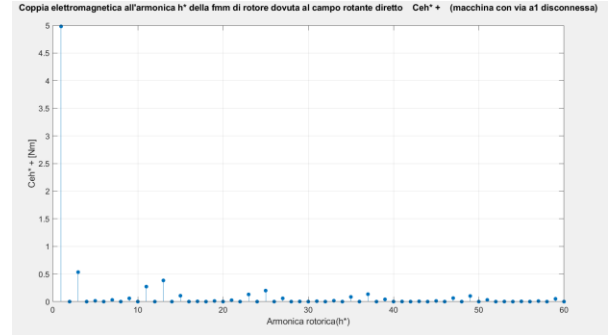


Figure 21: Torque spectrum C_{eh}^{*+} (machine without one parallel path)

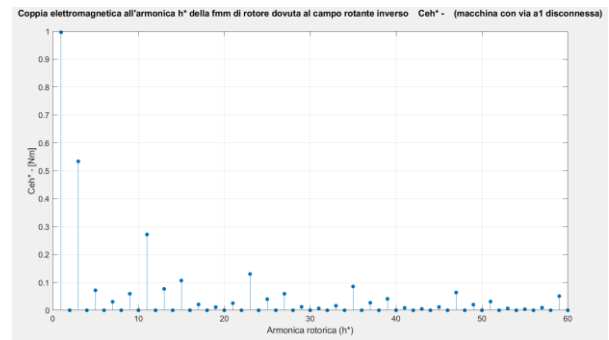


Figure 22: Torque spectrum C_{eh}^{*-} (machine without one parallel path)

In case of three parallel paths symmetrically disconnected between all phases, see Figures 23,24.

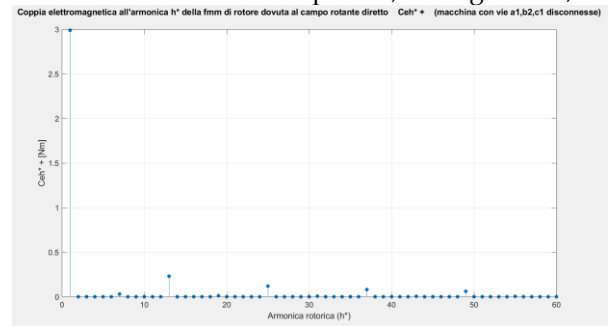


Figure 23: Torque spectrum C_{eh}^{*+} (machine with three parallel paths symmetrically disconnected)

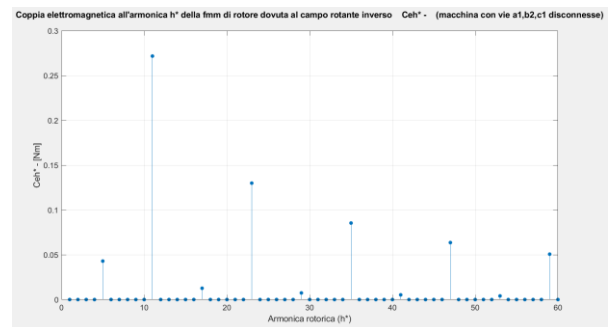


Figure 24: Torque spectrum C_{eh}^{*-} (machine with three parallel paths symmetrically disconnected)

The torque harmonics $C_{eh^*}^+$ and $C_{eh^*}^-$ are illustrated in function of the rotor harmonic index h^* , but the harmonic for $h^* = 1$ is the one that is desired to be constant in time.

Overall, Figures 19-24 show that the harmonic C_{e1}^+ (i.e. average value of the torque C_e) reduces disconnecting more parallel paths, instead the torque ripple increases if the parallel paths are not disconnected symmetrically.

In case of symmetrical disposition of parallel paths connected, the torque C_{e1} is constant instead if only one parallel path is disconnected, the torque C_{e1} is not constant since the two harmonics C_{e1}^+ and C_{e1}^- are different from zero.

10. Conclusions

Through the methodology presented in this thesis, it was possible to obtain the total electromagnetic torque expression in function of time t , seen as composition of more torque harmonics.

11. Bibliography

References

- [1] J. Zhang, W. Zhan, M. Ehsani: Fault-Tolerant Control of PMSM With Inter-Turn Short-Circuit Fault, IEEE Transactions on Energy Conversion, vol. 34, 2019, pp. 123-130.
- [2] J. Hang, S. Ding, X. Ren, Q. Hu: Integration of Interturn Fault Diagnosis and Torque Ripple Minimization Control for Direct-Torque-Controlled SPMSM Drive System, IEEE Transactions on Power Electronics, vol. 36, NO.10, 2021, pp. 11124-11134 .
- [3] G. Forstner, A. Kugi, W. Kemmtmüller: Fault-tolerant torque control of a three-phase permanent magnet synchronous motor with inter-turn winding short circuit, Elsevier Control Engineering Practice, vol. 113, 2021, pp. 1-11.
- [4] S. Cheng , R. Zhou, Z. Li: Robust Model-Free Fault-Tolerant Predictive Control for PMSM Drive System, IEEE Access, vol. 11, 2023, pp. 1-10.
- [5] M. Hedef, M.R. Mekideche, A. Djerdir: Vector Controlled Permanent Magnet

Synchronous Motor (PMSM) Drive with Stator Turn Fault, XIX International Conference on Electrical Machines - ICEM 2010, Rome, Italy, 7-10 Sept. 2010.

[6] V. Lešić, M. Vašak, T. M. Wolbank: Fault-tolerant Control of Permanent Magnet Synchronous Generator in Wind Turbines, Conference: European Wind Energy Association 2014 Annual Event, EWEA 2014, 2014.

[7] Foitzik, S., Doppelbauer, M.: Fault tolerant control of a three-phase PMSM by limiting the heat of an inter-turn fault. IET Electr. Power Appl. 1–11 (2021). <https://doi.org/10.1049/elp2.12142>

[8] S. Wei, S. Huang, J. Gao: Research on the Internal Short Circuit Fault Tolerant Operation of the PMSM, ITEC Asia-Pacific 2014, 2014.

[9] https://castellidezza.faculty.polimi.it/wp-content/uploads/Azionamenti-brushless_w.pdf

[10] Fitzgerald, Kingsley, Umans: Electric Machinery, sixth edition, McGraw-Hill Companies

[11] Correggiari, Di Gerlando, Foglia: Lecture Notes of Construction and Design of Electrical Machines

12. Acknowledgements

I express my sincere gratitude to Dr. Eng. Matteo Deponti for his invaluable support during the arduous task of verifying the calculations and, more generally, for his constant presence throughout the writing of this paper.

A special acknowledgement goes to Professor Perini for his thorough review of the content of this thesis and for ensuring the correctness of the methodology presented.